Controlled Rod Nanostructured Assembly of Diphenylalanine and Their Optical Waveguide Properties

Qi Li,[†,‡] Yi Jia,[*,†] Luru Dai,[‡] Yang Yang,[‡] and Junbai Li[*,†,‡]

[†]Beijing National Laboratory for Molecular Sciences, CAS Key Lab of Colloid, Interface and Chemical Thermodynamics, Institute of Chemistry, Chinese Academy of Sciences, Beijing 100190, China and [‡]National Center for Nanoscience and Technology, Beijing 100190, China

ABSTRACT Diphenylalanine (FF) microrods were obtained by manipulating the fabrication conditions. Fourier transform infrared (FTIR), circular dichroism (CD), fluorescence (FL) spectroscopy, and X-ray diffraction (XRD) measurements revealed the molecular arrangement within the FF microrods, demonstrating similar secondary structure and molecular arrangement within FF microtubes and nanofibers. Accordingly, a possible mechanism was proposed, which may provide important guidance on the design and assembly manipulation of peptides and other biomolecules. Furthermore, characterization of a single FF microrod indicates that the FF microrod can act as an active optical waveguide material, allowing locally excited photoluminescence to propagate along the length of the microrod with coupling out at the microrod tips.

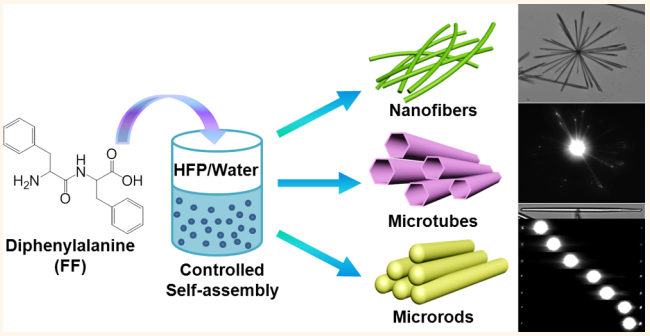

KEYWORDS: diphenylalanine · self-assembly · microrod · microtube · nanofiber

The self-assembly of nanomaterials to form well-ordered hierarchical structures provides great opportunities in optical, electronic, and magnetic materials and devices.[1−4] In the past decades, great efforts have been focused on self-assembly of peptide molecules owing to their structural simplicity, biocompatibility, chemical versatility, facile synthesis, and widespread applications.[5,6] Assembly could be effectively achieved by hydrogen bonding, electrostatic, hydrophobic, and $\pi-\pi$ stacking interactions. One well-known and the simplest peptide building block is diphenylalanine (FF), the core recognition motif of the Alzheimer's β-amyloid polypeptide. In different solvents and surfaces, FF could readily self-assemble into nanotubes (NTs),[7,8] microtubes (MTs),[9] nanowires (NWs),[10,11] nanovesicles (NVs),[12] *etc*. The polymorphism of FF-based assembly can be influenced and easily controlled by the experimental conditions such as solvents, peptide concentrations, pH, and temperature. For example, our group has previously demonstrated that the reversible transition between NTs and NVs can be simply achieved by adjusting the peptide concentration.[13] Ihee and co-workers realized NT and NW morphology control through manipulating the free-water content in the reaction medium.[10] A next and crucial step to make use of these structures is the quantitative control of the assembly to obtain solutions, with pure morphology and free of defects, and studying their function.

In this context, the self-assembly of FF into nanofibers (NFs), microtubes (MTs), and microrods (MRs) was conducted, as shown in Scheme 1. By controlling the preparation condition, such as ultrasonication time, the amounts of FF, and HFP/water ratio, MRs could be exclusively obtained. The obtained FF MRs possess single-crystalline structure, smooth surfaces, and flat end facets. More interestingly, such assembled FF MRs exhibit an excellent optical waveguide property, which is rarely observed in biological molecules.

RESULTS AND DISCUSSION

In a typical experiment, 1 mg of FF was first dissolved in 30 μL of HFP, then 120 μL of

* Address correspondence to jbli@iccas.ac.cn.

Received for review November 12, 2014 and accepted March 11, 2015.

Published online March 11, 2015
10.1021/acsnano.5b00623

water was poured into the above solution followed by ultrasonic treatment at room temperature for 5 min. Figure 1 shows scanning electron microscopy (SEM) images and transmission electron microscopy (TEM) images of the obtained FF assemblies with FF NFs (Figure 1b), MTs (Figure 1c,e), and MRs (Figure 1d,f). It has previously been reported that FF can be self-assembled in aqueous solution into NFs, NTs, NWs, or MTs.[8,10,14,15] However, FF rod structure has scarcely been reported. The obtained MRs are 30−100 μm in length and 2−3 μm in diameter. TEM demonstrated their solid structure (Figure 1f) compared to the hollow structure of MTs (Figure 1e). The selected area electronic diffraction pattern of FF MRs showed a pattern similar to that of FF MTs, indicating similar molecular arrangement and single-crystalline structure of MRs and MTs.

To gain better insight into the molecular organization of the FF MRs and exclusively obtain FF MRs, preparation parameters were varied, and the obtained products were analyzed on the molecular level by Fourier transform infrared (FTIR), circular dichroism (CD), fluorescence (FL) spectroscopy, and X-ray diffraction (XRD).

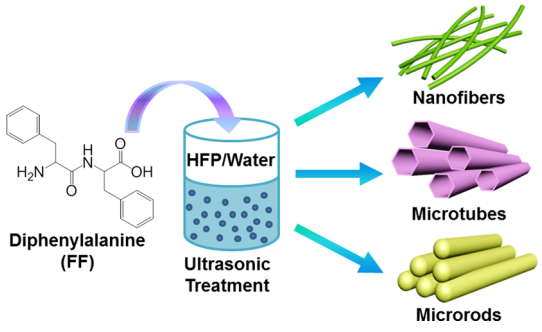

Scheme 1. Self-Assembly of FF into Nanofibers, Microtubes, and Microrods

Sonication proved to be indispensable for the formation of well-defined crystals, as it promotes crystallite homogeneity.[16,17] It is done routinely during sample crystallization and is liable to result in the formation of solid, nontubular crystals.[18] This is because sonication reduces or eliminates the concentration gradients across growing crystal faces that are necessary for tubular crystal formation.[19] Here, different ultrasonication times were set to manipulate the assembly of FF, as shown in Figure 2. At 1 min, both NFs and MTs were formed *via* molecular self-assembly of FF (Figure 2a,b). When the ultrasonication time was set as 5 min, FF mainly assembled into MTs, accompanied by small amounts of NFs and MRs (Figure 2c,d). As the ultrasonication time increased to 20 min, FF MRs were the predominant products, mingling with some FF MTs (Figure 2e,f). This result demonstrates that ultrasonication time influences the assembly of FF, and longer ultrasonication time (20 min) facilitates the formation of FF MRs. FTIR spectra (Figure 3a) of all FF assemblies obtained with different ultrasonication time show the characteristic peak of the amide I band at 1605 cm^{-1}, corresponding to a β-sheet secondary structure.[15] XRD patterns (Figure 3b) also demonstrate similar crystal structure of MTs and MRs, which is also very similar to the previously reported hexagonal structure of FF single crystals.[20] The same patterns were also found in CD and FL spectra (Figure 3c,d). As shown in Figure 3c, the CD spectra of all assemblies obtained with different ultrasonication time yield features similar to the β-sheet arrangement of FF molecules, with a negative band near 233 nm ($n-\pi^*$ transition).[21−23] For the FL spectra, all assemblies have an emission peak around 286 nm with an excitation wavelength of 259 nm (Figure 3d). No peak shift was observed compared to free FF molecules, indicating that no strong $\pi-\pi$ interactions occur between the aromatic residues. This is consistent with the spectra of MTs

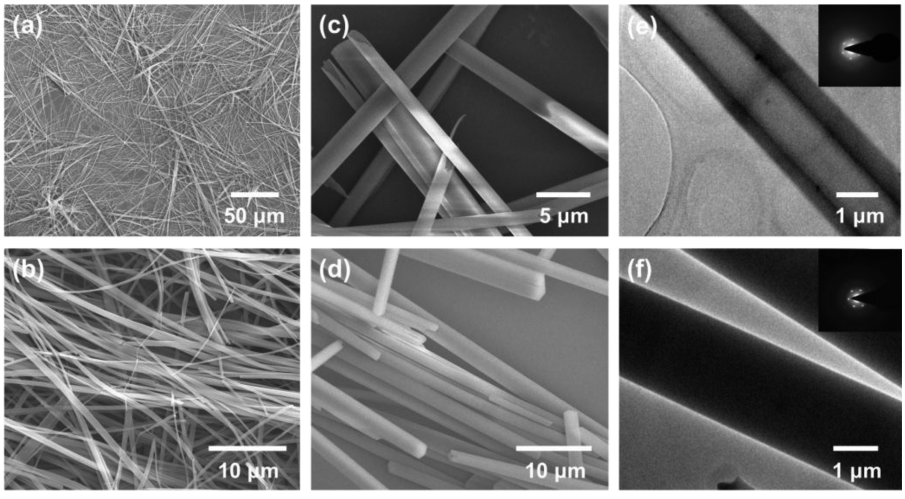

Figure 1. SEM images of FF assemblies (a), nanofibers (b), microtubes (c), and microrods (d), and TEM images of FF microtube (e) and microrod (f) (the inset is the selected area electronic diffraction pattern of microtube and microrod).

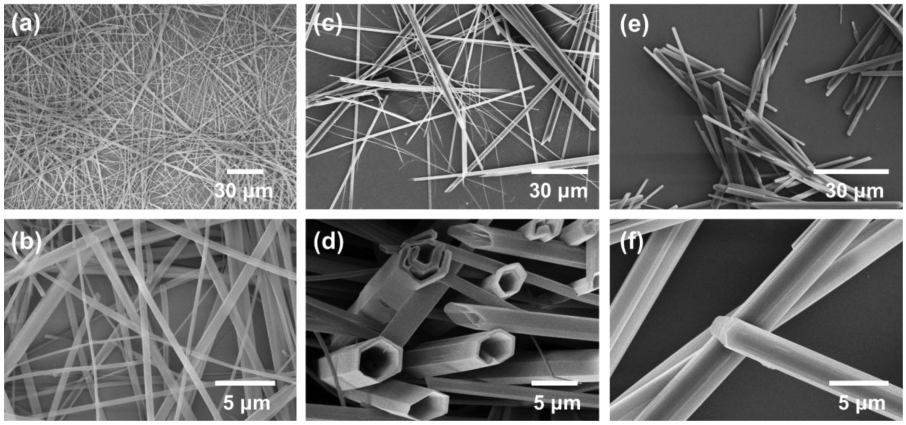

Figure 2. SEM images of 1 mg of FF assembled in HFP/water (30 μL/120 μL) solutions with different ultrasonication time, (a,b) 1 min, (c,d) 5 min, (e,f) 20 min.

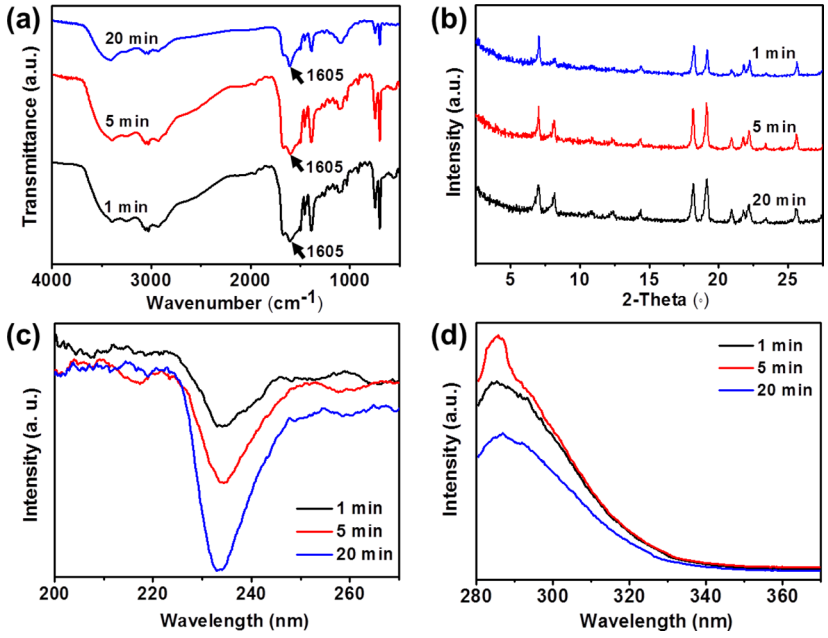

Figure 3. FTIR spectra (a), XRD patterns (b), CD spectra (c), and FL spectra (d) of FF assembly obtained with different ultrasonication time.

reported in previous research,[15] further confirming similar crystal structure of MRs compared to MTs. Therefore, despite the difference in their morphologies, the molecular arrangement in FF MRs is nearly identical to that of MTs or NFs.

The concentration has been reported to exert a huge influence on the assembly morphology by changing the speed of crystallization. High concentration can accelerate the assembly process and a large number of solid rod-like products can be formed in the solution.[16] In this work, different amounts of FF (1−4 mg) were chosen to assemble in HFP/water (30 μL/120 μL) solutions with ultrasonic treatment at room temperature for 20 min. It can be seen in Figure 4a that 1 mg of FF assembled in HFP/water solutions forms a substantial fraction of FF MRs, mixing with small amounts of MTs, scarcely any NFs. This result is consistent with those obtained by adjusting the ultrasonication time (Figure 2e,f). When the amounts of FF increased to 2, 3, and 4 mg, the obtained assembly was almost entirely FF MRs with the average diameter of 2 μm (Figure 4b−d). This result indicates that self-assembly of FF is significantly dependent on the concentration, similar to the assembly of nanotubes or nanowires.[10,24] With increasing peptide concentration and optimized ultrasonication time, solid MRs instead of hollow MTs were formed. FTIR and FL spectra (Figure 5) of these assemblies obtained with different amounts of FF possess similar peaks, further confirming similar molecular arrangement of MTs and MRs. Although the organization of the crystals remained the same, a small shift in the peak positions toward smaller angles was observed in the FF MRs diffractogram with increased amounts of FF (Figures 5b and S1), indicating that the lattice parameters suffered a slight alteration. Similar behavior has also been observed previously in FF NTs

and FF NWs,[10] which suggests that the free-water content plays an important role. Higher FF concentration makes the assemblies water deficient and leads to lattice expansion in the crystalline unit cell structure as a result of the reduced interactions between water and FF molecules.[25] Besides XRD patterns, the CD spectra of the assembly obtained with different amounts of FF also changed with increased amounts of FF (Figure 5c), shifting from 228 nm for the crystals obtained from 1 mg of FF to 235 nm for those obtained from 4 mg of FF. This phenomenon could be attributed to the increased degree of β-sheet twisting as the concentration increases.[26]

Aside from ultrasonic time and the amounts of FF, solvent environment is surely another key factor in directing FF self-assembly.[27−29] Here, the influence of the HFP/water volume ratio of the solution on the FF assembly morphology was studied. As an optimized condition for MR formation, 3 mg of FF was chosen to assemble in different HFP/water solution with ultrasonic treatment at room temperature for 20 min. It can be observed from Figure 6 that when the HFP/water ratios are 10 μL/140 μL and 30 μL/120 μL, FF were mainly assembled into MRs (Figure 6a,b); while the content of HFP increased to almost half of that of the solution, MTs were the predominant products with some NFs (Figure 6c). Upon further increasing the HFP content to 90 μL, substantial amounts of NFs were mainly observed in addition to some hollow microtubes (Figure 6d). However, as the ratio of HFP increased to 11:4, no aggregation could be obtained (Figure S2). This behavior may be attributed to high hydrogen bonding ability of HFP, which form stable intermolecular hydrogen bonds with FF molecules, leading to the solvation of FF. In this case, it is difficult for the FF to migrate out of their solvation shells to form aggregates.[30] When this peptide solution was deposited on a silicon wafer, the evaporation of HFP promoted the self-assembly of FF to form microtubes, clusters, or amorphous structures (Figure S3).

From the above results, one can conclude that higher concentration, longer ultrasonication time, and appropriate HFP/water volume ratio are crucially important for the formation of MR. It has been reported in previous work that FF MTs were obtained by growth of the assembled nanotube seeds.[15,31] According to the above molecular level analysis by FTIR, CD, FL spectroscopy, and XRD analysis, the FF MRs may also be obtained through this way, if a higher concentration, longer ultrasonication time, and appropriate HFP/water ratio is adopted. In this case, we propose

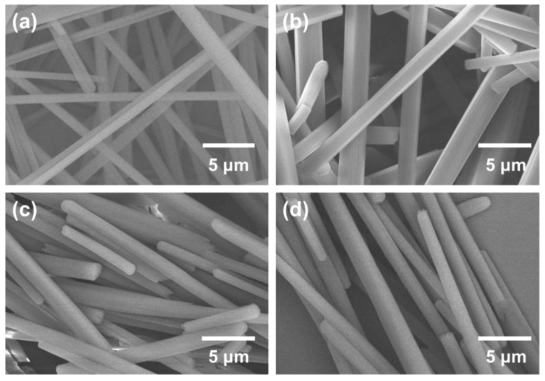

Figure 4. SEM images of (a) 1 mg, (b) 2 mg, (c) 3 mg, and (d) 4 mg of FF assembled in HFP/water (30 μL/120 μL) solutions with ultrasonic treatment at room temperature for 20 min.

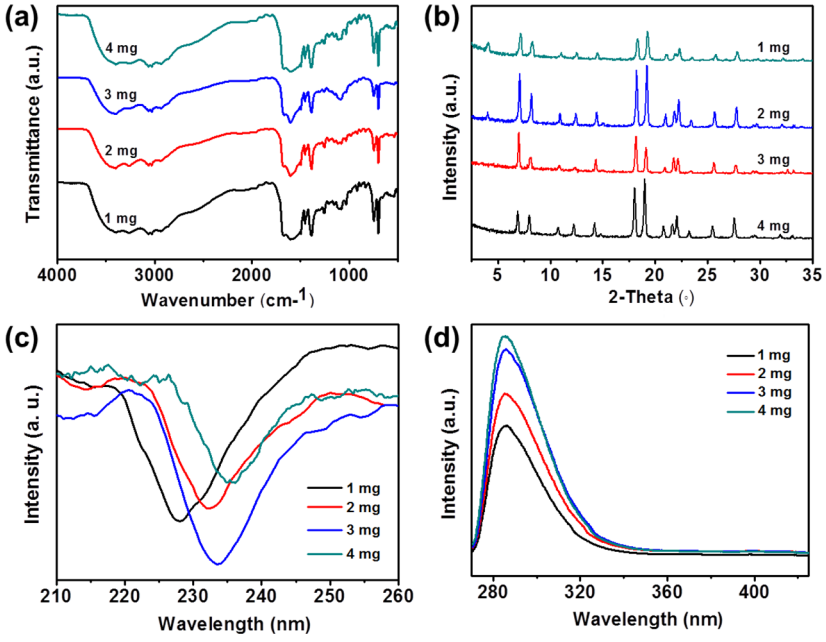

Figure 5. FTIR spectra (a), XRD patterns (b), CD spectra (c), and FL spectra (d) of FF assembly obtained with different amounts of FF.

that the FF molecules first self-assemble into nanotube in the presence of water, and then reorganize with the driving force of sonication and grow into microrods through hydrogen bonding and hydrophobic interactions between FF aromatic residues.[15] As for the different morphologies, the nucleation and growth of the nucleated clusters are directly related to the conditions of self-assembly. For the formation of FF MRs, a higher concentration was adopted to accelerate the assembly process and make the whole assemblies lack water; therefore, the hydrogen bond interactions between water and FF molecules are reduced.[25] As a consequence, the growth along the wall is almost the same as that in the middle of the nucleated clusters.[32] The 1-D rod-like structure was then formed. Longer ultrasonication time eliminates the concentration gradients across growing crystal faces and promotes crystallite homogeneity, which is also the indispensable condition for the formation of solid nontubular crystals.[16,33] Besides, an appropriate HFP/water volume ratio is vital for FF MR construction, which determines the nucleation and crystal growth rate of FF. For example, as the volume of HFP increases, the morphology of FF assembly changes from MRs to MTs and NFs. This phenomenon is ascribed to the decreased supersaturation and nucleation of FF molecules. Although the concentration of FF is not changed, the crystallization rate of FF is reduced as the amount of HFP increases.[29]

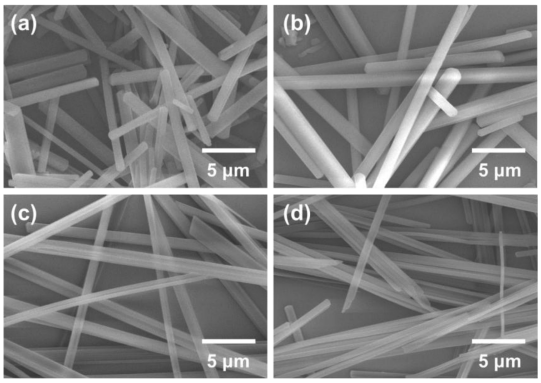

Figure 6. SEM images of 3 mg of FF assembled in different volume ratios of HFP/water solutions with ultrasonic treatment at room temperature for 20 min: (a) 10 μL/140 μL, (b) 30 μL/120 μL, (c) 70 μL/80 μL, and (d) 90 μL/60 μL. The total solution volume is kept constant at 150 μL.

Since FF MRs possess smooth surfaces and crystal structures, they are desirable to be used as waveguide materials. To endow the FF MRs outstanding photonic properties, rhodamine B (RhB) was added into HFP/water solution and coassembled with FF. After doping with RhB, the assemblies still present the MR structure, without significant change in morphology (Figure 7a). Figure 7b presents XRD profiles from crystalline samples of bare FF MRs and FF-RhB MRs. One observes that the XRD pattern does not significantly change after doping. This implies that the addition of RhB does not alter the molecular arrangement of the peptide assemblies.[34]

The waveguide property of FF-RhB MR was then investigated by local illumination microscopy with individual assemblies (Figure 8a). When excited at one end, a bright photoluminescence (PL) spot is observed at the other end of the microrod, with the rod body emitting nearly no PL (Figure 8b). If the excited point is moved to the middle part, bright PL spots are observed at both ends of the MR. This is a typical characteristics of optical waveguide, suggesting that FF-RhB MR can act as an optical waveguide material.[35] Furthermore, the distance-dependent PL intensity at each end of the FF-RhB MR was measured.[36,37] As shown in Figure 8c, the out-coupled light decreases almost exponentially with the increase in propagation distance with an attenuation length of about 40 μm. The waveguide losses in the FF-RhB MR can be attributed to scattering and coupling between the MR and substrate.[32,35] These results demonstrate that the FF-RhB MRs can act as potential optical waveguide materials, although the attenuation length still has to be increased by further improving the crystalline quality.

Similarly, FF-RhB MTs were prepared and investigated by local illumination microscopy. As shown in Figure 9, when exciting at the intersections of crossed MTs, bright PL spots were observed at the other end of all the MTs with weaker emission observed along the MTs bodies. It indicates that those MTs are also able to absorb the excitation light and propagate the PL

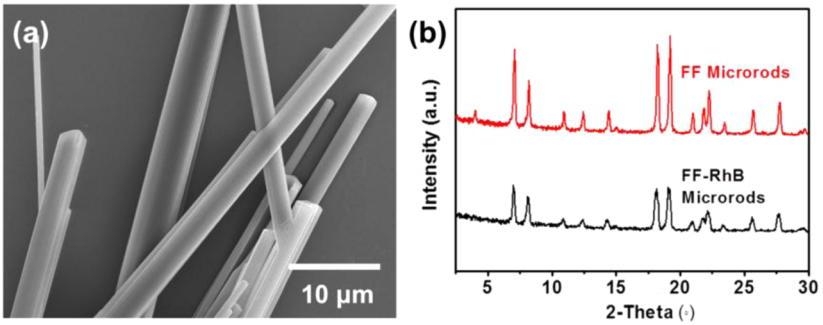

Figure 7. SEM image (a) of FF-RhB MR, and XRD patterns (b) of FF MRs and FF-RhB MRs.

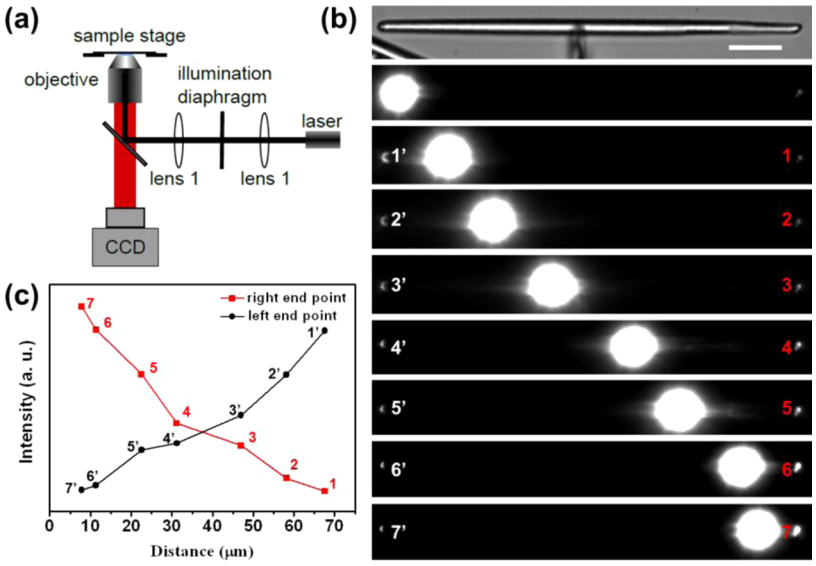

Figure 8. Schematic illustration of the experimental setup used for optical waveguide measurement (a). Bright-field image and PL images (b) of a single FF-RhB MR when translating the excitation spot along the MR from left to right; the excited wavenumber is 561 nm and scale bar is 10 μm. The excitation distance-dependent PL intensity at each end point (c); the distance denotes the length between right end point and excitation spot.

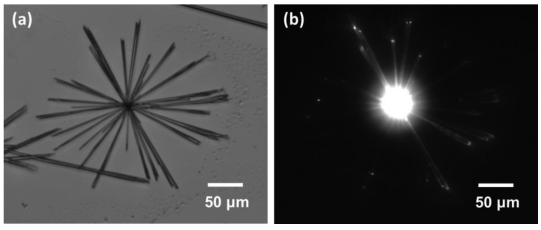

Figure 9. Bright field image (a) and PL image of FF-RhB MTs (b) excited at 561 nm.

emission toward tips, demonstrating good waveguide property of the MTs. The distance-dependent PL intensity at the end of a single FF-RhB MT was also measured (Figure S4). The out-coupled light was also shown to decrease exponentially with the increase in propagation distance, and the attenuation length is about 80 μm. Compared to the solid FF-RhB MR, the FF-RhB MT demonstrates lower waveguide loss during the propagation of light. Such an optical loss in the FF-RhB MT shall be ascribed to the reabsorption, while the optical loss for the FF-RhB MR is due to the scattering and coupling between the MR and the substrates.[35]

CONCLUSIONS

In summary, FF MRs were obtained by simply changing the fabrication conditions, such as ultrasonication time, the amounts of FF, and HFP/water volume ratio. The influences of these parameters in directing the assembly morphology of FF were studied in detail. FTIR, CD, FL spectra, and XRD patterns demonstrate that FF MRs contain similar secondary structure and molecular arrangement compared to FF MTs and NFs. Accordingly, a possible mechanism was proposed, which may provide important guidance on the design and assembly manipulation of peptides and other biomolecules. Furthermore, RhB introduction into FF MRs and MTs yield fluorescent MRs and MTs, and both of them have good optical waveguide properties.

METHODS

Materials. The lyophilized diphenylalanine (H-Phe-Phe-COOH, FF) was purchased from Bachem (Budendorf, Switzerland). 1,1,3,3,6,6-Hexafluoro-2-propanol (HFP) was obtained from Aladdin. Rhodamine B was purchased from Sigma-Aldrich. The water used in all experiments was prepared in a three-stage Millipore Milli-Q plus 185-purification system and had a resistivity higher than 18.2 MΩ. All reagents above were used without further purification.

Preparation of FF Nanofibers, Microtubes, and Microrods. In a typical experiment, 1 mg of FF powders were first dissolved in 30 μL of 1,1,1,3,3,3,-hexafluor-2-propanol (HFP). Then 120 μL of water was poured into the above solution and ultrasonically treated at room temperature for 5 min. The obtained white precipitate formed at the bottom was used for further characterization.

Characterization. The samples were characterized by scanning electron microscopy (SEM, Hitachi S-4800) and transmission electron microscopy (TEM, JEOL JEM-1011). The selected area electronic diffraction pattern was obtained by a Philips CM200-FEG transmission electron microscope. The precipitate was dried under vacuum and then pressed into a KBr pellet for FTIR (Bruker TENSOR-27) spectroscopy measurement. X-ray diffraction (XRD) patterns were measured at 25 °C using Rigaku. Data were collected on a Rigaku D/max 2500 instrument equipped with a Cu filter under the following conditions: scan speed, 2°/min; Cu Kα radiation, λ = 1.5405 Å. Circular dichroism (CD) spectra were monitored with a JASCO J-810 spectropolarimeter at room temperature between 190 and 300 nm. Fluorescence (FL) spectra were scanned from 270 to 400 nm at an emission wavelength of 259 nm using a F-4500 fluorescence spectrophotometer. The optical waveguide

property of MRs was tested by self-assembled local illumination microscopy.

Conflict of Interest: The authors declare no competing financial interest.

Acknowledgment. The authors acknowledge the financial support from the National Nature Science Foundation of China (Project No. 21433010, 21320102004, 91027045, 21303221 and 21273053), National Basic Research Program of China (973 program, 2013CB932800).

Supporting Information Available: Figures S1–S4. This material is available free of charge *via* the Internet at http://pubs.acs.org.

REFERENCES AND NOTES

1. Ariga, K.; Mori, T.; Hill, J. P. Mechanical Control of Nanomaterials and Nanosystems. *Adv. Mater.* **2012**, *24*, 158–176.
2. Ariga, K.; Ji, Q.; Mori, T.; Naito, M.; Yamauchi, Y.; Abe, H.; Hill, J. P. Enzyme Nanoarchitectonics: Organization and Device Application. *Chem. Soc. Rev.* **2013**, *42*, 6322–6345.
3. Russell, J. T.; Lin, Y.; Böker, A.; Su, L.; Carl, P.; Zettl, H.; He, J.; Sill, K.; Tangirala, R.; Emrick, T.; Littrell, K.; Thiyagarajan, P.; Cookson, D.; Fery, A.; Wang, Q.; Russell, T. P. Self-Assembly and Cross-Linking of Bionanoparticles at Liquid–Liquid Interfaces. *Angew. Chem., Int. Ed.* **2005**, *44*, 2420–2426.
4. Dabkowska, A. P.; Niman, C. S.; Piret, G.; Persson, H.; Wacklin, H. P.; Linke, H.; Prinz, C. N.; Nylander, T. Fluid and Highly Curved Model Membranes on Vertical Nanowire Arrays. *Nano Lett.* **2014**, *14*, 4286–4292.
5. Gazit, E. Self-Assembled Peptide Nanostructures: The Design of Molecular Building Blocks and Their Technological Utilization. *Chem. Soc. Rev.* **2007**, *36*, 1263–1269.
6. Yan, X. H.; Zhu, P. L.; Li, J. B. Self-Assembly and Application of Diphenylalanine-Based Nanostructures. *Chem. Soc. Rev.* **2010**, *39*, 1877–1890.
7. Vasudev, M. C.; Koerner, H.; Singh, K. M.; Partlow, B. P.; Kaplan, D. L.; Gazit, E.; Bunning, T. J.; Naik, R. R. Vertically Aligned Peptide Nanostructures Using Plasma-Enhanced Chemical Vapor Deposition. *Biomacromolecules* **2014**, *15*, 533–540.
8. Gan, Z.; Wu, X.; Zhu, X.; Shen, J. Light-Induced Ferroelectricity in Bioinspired Self-Assembled Diphenylalanine Nanotubes/Microtubes. *Angew. Chem., Int. Ed.* **2013**, *52*, 2055–2059.
9. Adler-Abramovich, L.; Aronov, D.; Beker, P.; Yevnin, M.; Stempler, S.; Buzhansky, L.; Rosenman, G.; Gazit, E. Self-Assembled Arrays of Peptide Nanotubes by Vapour Deposition. *Nat. Nanotechnol.* **2009**, *4*, 849–854.
10. Kim, J.; Han, T. H.; Kim, Y.-I.; Park, J. S.; Choi, J.; Churchill, D. C.; Kim, S. O.; Ihee, H. Role of Water in Directing Diphenylalanine Assembly into Nanotubes and Nanowires. *Adv. Mater.* **2010**, *22*, 583–587.
11. Ryu, J.; Kim, S. W.; Kang, K.; Park, C. B. Synthesis of Diphenylalanine/Cobalt Oxide Hybrid Nanowires and Their Application to Energy Storage. *ACS Nano* **2010**, *4*, 159–164.
12. Guo, C.; Luo, Y.; Zhou, R.; Wei, G. Probing the Self-Assembly Mechanism of Diphenylalanine-Based Peptide Nanovesicles and Nanotubes. *ACS Nano* **2012**, *6*, 3907–3918.
13. Yan, X. H.; Cui, Y.; He, Q.; Wang, K. W.; Li, J. B.; Mu, W. H.; Wang, B.; Ou-yang, Z. C. Reversible Transitions between Peptide Nanotubes and Vesicle-Like Structures including Theoretical Modeling Studies. *Chem.—Eur. J.* **2008**, *14*, 5974–5980.
14. Na, N.; Mu, X.; Liu, Q.; Wen, J.; Wang, F.; Ouyang, J. Self-Assembly of Diphenylalanine Peptides into Microtubes with "Turn On" Fluorescence Using an Aggregation-Induced Emission Molecule. *Chem. Commun.* **2013**, *49*, 10076–10078.
15. Yan, X. H.; Li, J. B.; Möhwald, H. Self-Assembly of Hexagonal Peptide Microtubes and Their Optical Waveguiding. *Adv. Mater.* **2011**, *23*, 2796–2801.
16. Zhao, Y. S.; Yang, W. S.; Yao, J. N. Organic Nanocrystals with Tunable Morphologies and Optical Properties Prepared through a Sonication Technique. *Phys. Chem. Chem. Phys.* **2006**, *8*, 3300–3303.
17. Wang, H. Q.; Yan, X. H.; Li, G. L.; Pilz-Allen, C.; Möhwald, H.; Shchukin, D. Sono-Assembly of Highly Biocompatible Polysaccharide Capsules for Hydrophobic Drug Delivery. *Adv. Healthcare Mater.* **2014**, *3*, 825–831.
18. Skorb, E. V.; Moehwald, H.; Irrgang, T.; Fery, A.; Andreeva, D. V. Ultrasound-Assisted Design of Metal Nanocomposites. *Chem. Commun.* **2010**, *46*, 7897–7899.
19. Eddleston, M. D.; Jones, W. Formation of Tubular Crystals of Pharmaceutical Compounds. *Cryst. Growth Des.* **2009**, *10*, 365–370.
20. Goerbitz, C. H. The Structure of Nanotubes Formed by Diphenylalanine, The Core Recognition Motif of Alzheimer's Beta-Amyloid Polypeptide. *Chem. Commun.* **2006**, 2332–2334.
21. Yan, X. H.; Cui, Y.; He, Q.; Wang, K. W.; Li, J. B. Organogels Based on Self-Assembly of Diphenylalanine Peptide and Their Application to Immobilize Quantum Dots. *Chem. Mater.* **2008**, *20*, 1522–1526.
22. Behanna, H. A.; Donners, J. J. J. M.; Gordon, A. C.; Stupp, S. I. Coassembly of Amphiphiles with Opposite Peptide Polarities into Nanofibers. *J. Am. Chem. Soc.* **2005**, *127*, 1193–1200.
23. George, J.; Thomas, K. G. Surface Plasmon Coupled Circular Dichroism of Au Nanoparticles on Peptide Nanotubes. *J. Am. Chem. Soc.* **2010**, *132*, 2502–2503.
24. Song, Y.; Challa, S. R.; Medforth, C. J.; Qiu, Y.; Watt, R. K.; Pena, D.; Miller, J. E.; Swol, F. v.; Shelnutt, J. A. Synthesis of Peptide-Nanotube Platinum-Nanoparticle Composites. *Chem. Commun.* **2004**, 1044–1045.
25. Wu, X. L.; Xiong, S. J.; Wang, M. J.; Shen, J. C.; Chu, P. K. Water-Sensitive High-Frequency Molecular Vibrations in Self-Assembled Diphenylalanine Nanotubes. *J. Phys. Chem. C* **2012**, *116*, 9793–9799.
26. Fry, H. C.; Garcia, J. M.; Medina, M. J.; Ricoy, U. M.; Gosztola, D. J.; Nikiforov, M. P.; Palmer, L. C.; Stupp, S. I. Self-Assembly of Highly Ordered Peptide Amphiphile Metalloporphyrin Arrays. *J. Am. Chem. Soc.* **2012**, *134*, 14646–14649.
27. Mason, T. O.; Chirgadze, D. Y.; Levin, A.; Adler-Abramovich, L.; Gazit, E.; Knowles, T. P. J.; Buell, A. K. Expanding the Solvent Chemical Space for Self-Assembly of Dipeptide Nanostructures. *ACS Nano* **2014**, *8*, 1243–1253.
28. Zhu, P. L.; Yan, X. H.; Su, Y.; Yang, Y.; Li, J. B. Solvent-Induced Structural Transition of Self-Assembled Dipeptide: From Organogels to Microcrystals. *Chem.—Eur. J.* **2010**, *16*, 3176–3183.
29. Su, Y.; Yan, X. H.; Wang, A. H.; Fei, J. B.; Cui, Y.; He, Q.; Li, J. B. A Peony-Flower-Like Hierarchical Mesocrystal Formed by Diphenylalanine. *J. Mater. Chem.* **2010**, *20*, 6734–6740.
30. Carny, O.; Shalev, D. E.; Gazit, E. Fabrication of Coaxial Metal Nanocables Using a Self-Assembled Peptide Nanotube Scaffold. *Nano Lett.* **2006**, *6*, 1594–1597.
31. Wang, M. J.; Du, L. J.; Wu, X. L.; Xiong, S. J.; Chu, P. K. Charged Diphenylalanine Nanotubes and Controlled Hierarchical Self-Assembly. *ACS Nano* **2011**, *5*, 4448–4454.
32. Chen, S.; Chen, N.; Yan, Y. L.; Liu, T.; Yu, Y.; Li, Y.; Liu, H.; Zhao, Y. S.; Li, Y. Controlling Growth of Molecular Crystal Aggregates for Efficient Optical Waveguides. *Chem. Commun.* **2012**, *48*, 9011–9013.
33. Perez-Hernandez, N.; Fort, D.; Perez, C.; Martin, J. D. Water-Induced Molecular Self-Assembly of Hollow Tubular Crystals. *Cryst. Growth Des.* **2011**, *11*, 1054–1061.
34. Silva, R. F.; Araujo, D. R.; Silva, E. R.; Ando, R. A.; Alves, W. A. L-Diphenylalanine Microtubes As a Potential Drug-Delivery System: Characterization, Release Kinetics, and Cytotoxicity. *Langmuir* **2013**, *29*, 10205–10212.
35. Zhao, Y. S.; Xu, J. J.; Peng, A. D.; Fu, H. B.; Ma, Y.; Jiang, L.; Yao, J. N. Optical Waveguide Based on Crystalline Organic Microtubes and Microrods. *Angew. Chem., Int. Ed.* **2008**, *47*, 7301–7305.
36. Schneider, C. A.; Rasband, W. S.; Eliceiri, K. W. NIH Image to Image J: 25 Years of Image Analysis. *Nat. Methods* **2012**, *9*, 671–675.
37. Abramoff, M. D.; Magalhaes, P. J.; Ram, S. J. Image Processing with Image J. *Biophotonics Int.* **2004**, *11*, 36–42.